Supporting Information for: Solubilization of PET in binary mixture of HFIP and DCM

Md Arifuzzaman,[a] Jan-Michael Y. Carrillo,[b] Tomonori Saito,[a] Bobby Sumpter,[b] and Changwoo Do,[c]

[a]*Chemical Sciences Division, Oak Ridge National Laboratory, Oak Ridge, TN 37831*

[b]*Center for Nanophase Materials Science , Oak Ridge National Laboratory, Oak Ridge, TN 37831*

[c]*Neutron Scattering Division, Oak Ridge National Laboratory, Oak Ridge, TN 37831*

E-mail: doc1@ornl.gov

S1 Thermodynamic Conditions and Consistency of Coarse-Grained Simulations

To assess the robustness of the observed behavior, we extended the CGMD simulations to include pressures $P^* = 0.15$, 0.30, 0.60, and 1.00, along with a broader range of HFIP mole fractions. These pressures are all significantly above the critical pressure of the LJ system with a cutoff of 2.5 σ, ensuring that the system remains liquid-like across all compositions studied.[1] Under these conditions, even though one of the pure components (DCM-like interaction strength) corresponds to a supercritical state when considered independently in reduced units, the mixture remains a condensed, liquid-like phase due to the elevated pressure. For comparison with the all-atom MD results, we focus primarily on the state point $P^* = 0.30$, as it reproduces the expected solvent quality ordering between HFIP and DCM.

In particular, $\langle R_g^2 \rangle$ in pure HFIP is greater than in pure DCM, consistent with HFIP acting as a better solvent for PET, as also observed in the all-atom MD simulations (see Fig. S1a).

We emphasize that the CGMD simulations are not intended to reproduce experimental thermodynamic state points through direct mapping of temperature, pressure, or density. Instead, the goal is to capture the relative interaction hierarchy between components (as defined by the LJ energy parameters in Table 1) and to probe the resulting structural and conformational trends. The simulations are therefore interpreted in a qualitative, mechanistic sense rather than as quantitatively predictive of experimental observables.

To assess consistency between coarse-grained and atomistic descriptions, additional analysis was performed on all-atom MD simulations. The radius of gyration, $\langle R_g^2 \rangle$, of a 10-monomer PET chain shows an increase from pure DCM to approximately 26% HFIP, (see Fig. S1a) followed by an oscillatory behavior at higher HFIP fractions. This composition corresponds to the onset of solvent clustering and a minimum in cluster density.

The CGMD simulations reproduce these qualitative trends across all pressures studied. The $\langle Rg^2 \rangle$ exhibits a maximum followed by oscillatory behavior as a function of HFIP composition (see Fig. S1b). For comparison, the all-atom configurations were mapped onto the coarse-grained representation using molecular centroids for HFIP and DCM and phenyl-ring centroids for PET. Partial radial distribution functions ($g(r)$) computed from the mapped trajectories show that HFIP forms distinct solvation shells around PET, whereas DCM is depleted in the vicinity of the polymer. (see Fig. S1c) Similarly, $g(r)$'s show preferential solvation of PET by HFIP and depletion of DCM, consistent with the all-atom results (see Fig. S1d). Quantitative differences in peak positions and amplitudes arise from the coarse-grained representation, including the use of uniform bead sizes.

Solvent structuring was further analyzed through the structure factor $S(q)$. For the mapped all-atom MD (AAMD) trajectories, $S(q)$ is plotted as a function of q in absolute units of Å^{-1} (Fig. S1e), whereas the CGMD results are plotted in reduced units of σ^{-1} (Fig. S1f). This difference reflects the different length scales of the two models: the AAMD

simulations retain atomistic molecular dimensions and can therefore be represented in real-space units, while the CGMD simulations use coarse-grained beads with the bead diameter σ as the fundamental length scale. For the same reason, the polymer dimensions are reported in Å^2 for AAMD and in σ^2 for CGMD in Fig. S1a and Fig. S1b, respectively. Thus, the AAMD and CGMD results are not compared through a direct quantitative mapping of q or length scales, but rather through their qualitative composition-dependent trends.

The low-q behavior of $S(q)$ also differs between the two representations. In the mapped AAMD data, the accessible q range is relatively limited by the finite size of the atomistic simulation box, and the low-q intensity decreases with increasing HFIP fraction. This decreasing low-q contribution in the mapped AAMD $S(q)$ is consistent with the experimental SANS data in Fig. 3a, where the fitted Ornstein–Zernike correlation length decreases monotonically with increasing HFIP content, indicating that HFIP-rich composition fluctuations become shorter-ranged as the mixture becomes more HFIP-rich. Therefore, the decreasing low-q feature in Fig. S1e supports the same physical interpretation obtained from the experimental SANS analysis. In contrast, the CGMD simulations access a broader reduced-q range and exhibit an apparent increase in the low-q contribution for some compositions. This difference arises from the coarse-grained representation and reduced thermodynamic state point, which enhance the contrast between HFIP-rich and DCM-rich domains and therefore amplify long-wavelength composition fluctuations. Consequently, the CGMD $S(q)$ should be interpreted as a qualitative indicator of solvent-domain formation rather than as a quantitatively mapped scattering function.

Despite these differences, both AAMD and CGMD show composition-dependent changes in $S(q)$ that are consistent with the formation of solvent microstructure in the HFIP/DCM mixtures. The AAMD result provides the closer comparison to the experimental SANS data because it is represented in absolute q units and shows a decreasing low-q contribution with increasing HFIP fraction, consistent with Fig. 3a. The CGMD result, although expressed in reduced units, supports the same mechanistic picture by showing that solvent clustering

and composition fluctuations evolve strongly with HFIP fraction and correlate with changes in PET chain dimensions.

Overall, while the CGMD simulations are not thermodynamically mapped to experimental conditions, they consistently reproduce the same mechanistic trends observed in all-atom simulations, namely the coupling between solvent microstructure and polymer conformation. This supports their use as a qualitative framework for interpreting solvent–polymer interactions in this system.

References

(1) Asano, Y.; Fuchizaki, K. Phase diagram of the modified Lennard-Jones system. *The Journal of Chemical Physics* **2012**, *137*.

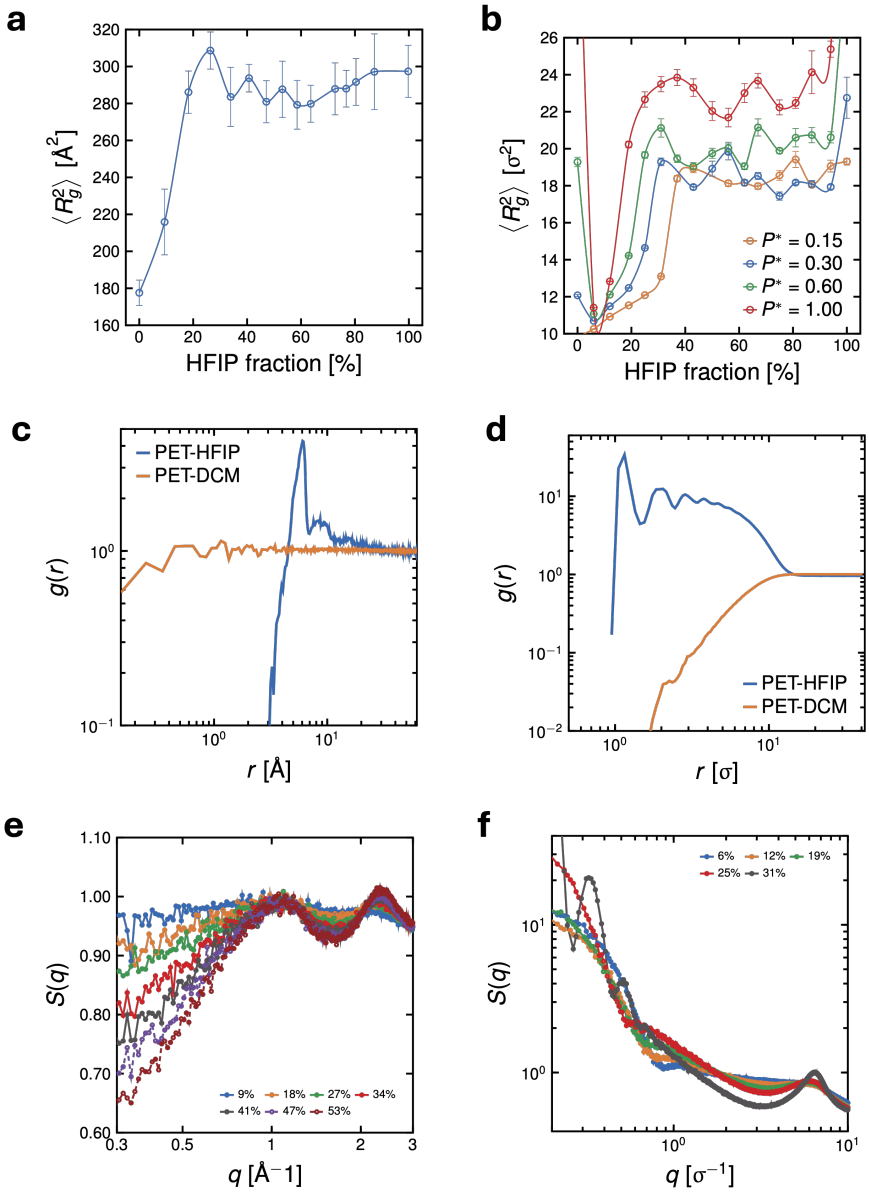

Figure S1: Dependence of the mean-squared radius of gyration, $\langle R_g^2 \rangle$, of PET chains on the HFIP fraction from all-atom MD simulations in Å^2 (a) and CGMD simulations in σ^2 (b), respectively. The CGMD simulations are performed at state points of $T^* = 1.0$ and varying P^*. Partial radial distribution functions, $g(r)$, between PET and HFIP/DCM from mapped all-atom MD simulations at 26% HFIP (c) and from CGMD simulations at $T^* = 1.0$, $P^* = 0.30$, and 25% HFIP (d). Scattering functions of HFIP, $S(q)$, from mapped all-atom MD simulations (e) and CGMD simulations (f) at varying %HFIP. The q-axis units and scaling are chosen separately for panels (e) and (f): the mapped AAMD $S(q)$ is shown in absolute units of Å^{-1} on a linear q-axis, whereas the CGMD $S(q)$ is shown in reduced units of σ^{-1} on a logarithmic q-axis to display the broader reduced-q range sampled in the coarse-grained simulations. The AAMD and CGMD $S(q)$ results are therefore compared in terms of qualitative composition-dependent trends rather than by direct quantitative mapping of q.